Journal of Applied Fluid Mechanics, Vol. 18, No. 6, pp. 1550-1562, 2025.
Available online at www.jafmonline.net, ISSN 1735-3572, EISSN 1735-3645.
https://doi.org/10.47176/jafm.18.6.3112

Experimental Investigation of Fuel Film Characteristics after Spray Impacting on Ultra-cold Surface

S. Jin[1], W. Zhang[1†], Z. Guo[1], Y. Yuan[1], J. Yan[1] and Y. Liu[2]

[1] *School of Mechanical Engineering, Beijing Institute of Technology, Beijing, 100081, China*
[2] *School of Mechanical Electronic and Information Engineering, China University of Mining and Technology-Beijing, Beijing, 100083, China*

†*Corresponding Author Email: zhangwz@bit.edu.cn*

ABSTRACT

In extremely cold environments, the phenomenon of spray impacting on surfaces is unavoidable and the fuel film attached to the surface is one of the crucial factors influencing emission, stability, and cold-start performance in internal combustion engines. However, there is currently a lack of research on the effects of spray impacting on ultra-cold surfaces. In this study, researchers investigated the effect of surface temperature on impinging spray and fuel film area with different values of injection pressure, injection duration, and surface roughness visually using backlight and scattering methods. The penetration and diameter of the impinging spray were not affected by the low surface temperature due to the ample momentum, whereas the height was slightly decreased at the ultra-cold surface. The fuel film area significantly decreased with the lower surface temperature and the shorter injection duration. An empirical correlation for the fuel film area was established for reflecting the relationship between the fuel film area and the low surface temperature or injection conditions. The decrease in fuel film area was more noticeable on the surface with lower temperature and higher surface roughness (Ra=17.69μm). Nevertheless, the longer injection duration weakened this decreasing trend. With the increasing number of injections, the fuel film area rose while the area on the ultra-cold surface, increased more slowly because of the higher viscosity and thickness of the previous residual film.

Article History

Received September 16, 2024
Revised November 30, 2024
Accepted January 3, 2025
Available online March 30, 2025

Keywords:

Spray impaction
Ultra-cold surface
Fuel film area
Empirical correlation
Surface roughness

1. INTRODUCTION

The phenomenon of liquid-phase spray impinging on surface is inevitable due to the poor atomization and evaporation results from miniaturization, low in-cylinder ambient temperature and pressure during the cold start of internal combustion (IC) engines (Schünemann et al., 1998; Hwang et al., 2015; Shi et al., 2020a). Although the impinging process is beneficial for secondary atomization, the fuel film formed may cause a misfire, deterioration of combustion, and emission issues (Suh et al., 2007; Zhu et al., 2014; Shi et al., 2020b; Zhang et al., 2023). Once proper combustion conditions are reached again, the fuel accumulated in multiple cycles will burn on the surface, resulting in carbon deposition and even ablation (Abou et al., 1999; Zhao & Kaiser, 2018). The surface temperature, one of the key parameters in the cylinder, directly affects the fuel-air mixing, fuel film spreading and flame propagation (Cho et al., 2010; Wu et al., 2023). Especially for diesel engines relying on compression ignition (CI), characteristics of the fuel-air mixture and fuel film strongly determine the ignition stability, leading to the noise, vibration, and harshness (NVH) and reliability influenced by cold start performance (He et al., 2023).

Researchers have conducted numerous investigations to examine the effect of surface temperature on the microscopic droplet-wall interaction or the macroscopic spray-wall interaction (Schünemann et al., 1998; Egermann et al., 2002; Drake et al., 2003). Liu et al. (2018) used laser-Induced exciplex fluorescence (LIEF) to measure the distribution of the gas-phase and liquid-phase, revealing that the high-concentration regions were promoted with the surface temperature from 773K to 333K. Accordingly, the air-fuel mixture process was reduced with the lower wall temperature because of the weakened evaporation in the study of Meingast et al. (2000). However, Orugant et al. (2024) found that the impingement spray had an obvious cooling effect foe the

ignition-assistant (IA) through the transient compressible 3-D CFD simulations with new spray-wall interaction (SWI) models. For cold start conditions, the surface temperature not only affected the air-fuel mixture formation but also changed the characteristics of the fuel film (Pan et al., 2019; Chen et al., 2020). Liu et al. (2019a) studied the characteristics of the fuel film by laser-induced fluorescence (LIF) technique and demonstrated that the fuel film volume decreased with the higher surface temperature. Zhu et al. (2001) investigated the film thickness and area enhanced at lower surface temperatures by the KIVA 3V. The nucleate boiling of the fuel film appeared when the wall temperature reached a critical value, and the boiling intensity was strengthened with the increasing wall temperature (Liu et al., 2019b). Furthermore, the temperature of the in-cylinder surface is even closer to the ambient temperature when engines quickly start in a cold environment, and the fuel film is easily formed due to the impact of liquid-phase spray on the low-temperature surface. Pan et al. (2017) investigated the thickness and the area of the ethanol film using LIF. Their results unveil that the film became thicker and the adhered mass increased with lower fuel or surface temperature, even though the wetted area became smaller owing to the larger viscosity. The film mass loss via wave entrainment decreased with the lower surface temperature (Li et al., 2019), and this phenomenon was dominated by gas-liquid interfacial interactions.

As implied from the above literature, the surface temperature affects not only the air-fuel mixture formation but also the deposition mass, area, and thickness of the fuel film via the process of evaporation, film breakup, and nucleate boiling. In cold-start conditions within frigid regions, the temperature of the piston wall could be as low as -20 °C. These extreme conditions can lead to the interaction between the liquid fuel and the ultra-cold wall, thereby impacting the subsequent fuel-air mixing process (Pan et al., 2019). Since previous investigations mainly primarily focused on the effect of higher surface temperature, there is a lack of the ultra-cold surface.

Furthermore, the morphology analysis of the fuel film has been researched more compared to theoretical analysis. The fuel film was strongly influenced by injection conditions such as injection pressure and duration (Xiao et al., 2019; Wang et al., 2022). The surface roughness changed significantly with poor engine operation (Shi et al., 2022). Nonetheless, the effect of this factor was barely considered due to the limitations of optical measurements (Pan et al., 2017; He et al., 2020). The diesel engine is more likely to misfire during cold starts at low temperatures, contributing to the accumulation of fuel film. Therefore, it is valuable to study the fuel film influenced by the coupling of surface temperature with injection conditions, surface roughness, and injection times.

In our paper, researchers conducted visualization experiments of spray impacting on ultra-cold surfaces using shadowgraph and direct photography methods. were conducted using the shadowgraph and direct photography methods. A parameter matrix, including surface temperature, injection pressure, injection duration, surface roughness, and different spray times for spray-wall interaction and fuel film area, was analyzed. Besides, an empirical correlation was established to reflect the relationship between the fuel film area and surface temperature or injection conditions.

2. EXPERIMENTAL APPARATUS AND PROCEDURES

2.1 Experimental Setup

As illustrated in Fig. 1, the experimental setup consists of the common rail system, a high-speed imaging and data acquisition system, the customized cooling system and related auxiliary parts. The common rail system provides injection pressure, incorporating a high-pressure oil pump (BOSCH-CP3), a conventional rail with a pressure regulator, a single-hole injector (BOSCH-CRI-2) of 0.16mm diameter, and a fuel tank. The desired injection pressure is achieved by the oil pump driven by an inverter motor.

The impacting process between spray and surface was captured by two high-speed cameras (FASTCAM SA4, Photron and EoSens Cube7, MIKROTRON) with operated speed of 20,000 fps (Resolution 512×352) and 5000 fps (Resolution 560×466), respectively. A dysprosium lamp and diffusion plate were adopted to provide a more adequate illumination source throughout the impacting process. Additionally, our research group conducted information extraction on the images using the software PFV and MATLAB. The computer software allowed the controller to send out a step signal that can be transmitted to the injector and two high-speed cameras for initiating injection and image recording, respectively.

The customized cooling system was composed of consisted of a customized Peltier element, a cooling module, heat sinks, and a temperature control device. The Peltier element reduced the temperature by the control device with adjustable voltage, and the heat was transferred through a cooling module. The surface temperature was regulated by adjusting the voltage input to the Peltier element combined with a thermocouple. Al-Si alloy surface intercepted from a piston blank was placed on the cold surface of the Peltier element. The alloy surfaces were connected by a thermally conductive silicone to reinforce thermal conductivity. enhance thermal conductivity. The polyurethane insulation layer was added to the side of the alloy plate to lessen the side's heat dissipation and maintain a uniform temperature on the plate, reduce sides heat dissipation and maintain a uniform temperature on the plate, as shown as exhibited in Fig. 1. This method ensured the stable surface temperature and replaced easily replaced the impacted surface. The surface temperature was reduced curtailed to -30 °C at an ambient temperature of 20 °C by the cooling system. The surface temperature of the Al-Si alloy plate was measured by a T-type thermocouple (Omega, accuracy: ±0.1 K) and recorded by the temperature logger (DAQ-970A, Keysight). Furthermore, researchers removed the frost to eliminate the humidity effect by wiping the surface before experiments.

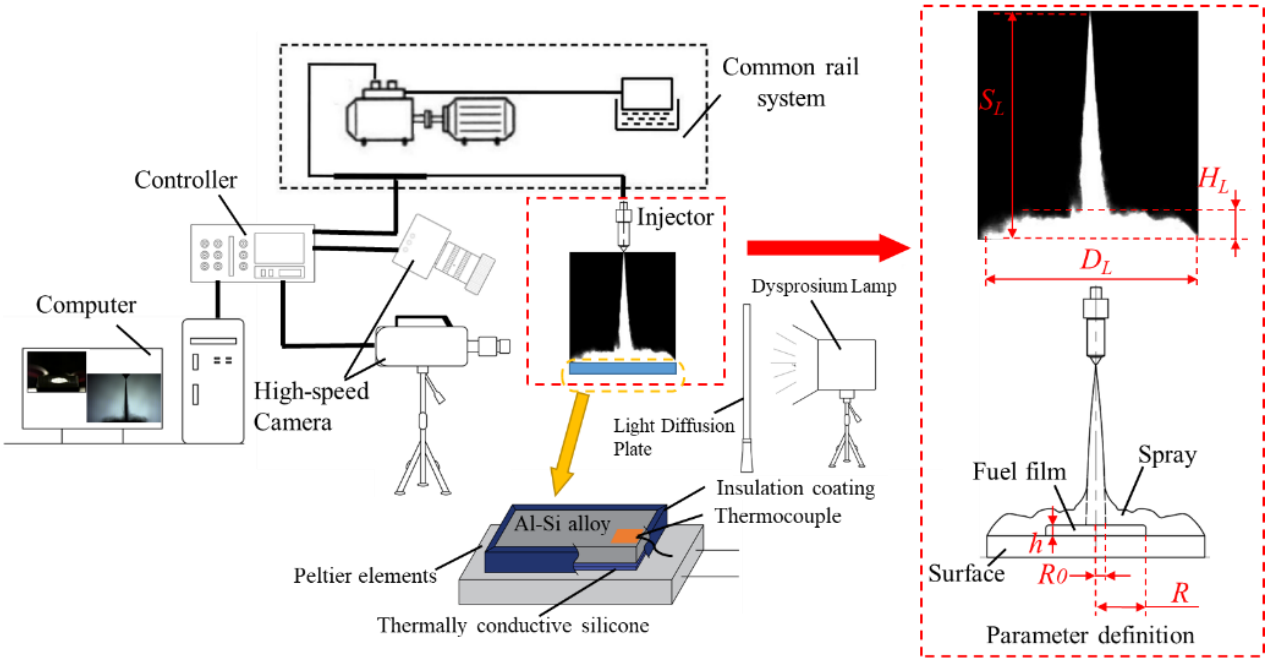

Fig. 1 Schematic diagram of the experimental setup

Table 1 Experimental conditions for impinging spray

Parameter	Value
Surface temperature (T_S, °C)	20, 0, -20
Surface roughness (Ra, μm)	1.12, 17.69
Injection pressure (P_i, MPa)	60, 80 (mainly)
Injection duration (t_i, ms)	1, 2, 3
Injection interval time (ms)	150

2.2 Experimental Parameter Setting

Table 1 shows that the test matrix determined several parameters such as surface temperature, injection pressure, injection period and surface roughness on the process after spray impacting on the ultra-cold surface. The spray impact process was captured by visual analysis of backlight and scattering. The image processing procedures are detailed in section 2.3. After processing section 2.3, our research group extracted useful information comprising penetration (P_L), diameter (D_L), and height (H_L) of the impacting spray. A schematic diagram of the spray parameters is presented in Fig. 1. The diameter represented the width of the oil spray and was defined as the distance between the two ends of the jet as the spray impinging on the wall. The height was obtained by measuring the distance from the highest spray after impingement to the lowest horizontal line of the wall. The penetration indicated the distance from the farthest end of the spray to the nozzle, and if the spray reached the wall, it was donated as P_L=S_L+D_L/2. The film spreading process changing with time is similar to the evolution process reported by Lamiel et al. (2021). Thus, the final fuel film, rather than the fuel film spreading process, demonstrated the effect of experimental parameters regarding the deposition of the fuel film.

The surface temperature (T_S, °C) was adjusted from -20 °C to 20 °C by the customized cooling system. This temperature reflected the actual wall temperature under low-temperature cold start conditions of IC engines. The fuel film formation was influenced by changes in surface roughness during the operation of IC engines. Our research group polished the surface of the alloy plate to two roughness levels (Ra = 1.12 μm and 17.69 μm) to better reveal the impact of roughness variations on the formation of thin films. The surface morphometry system (ST-400, NANOVEA) was employed to perform the surface condition, as presented in Fig. 2.

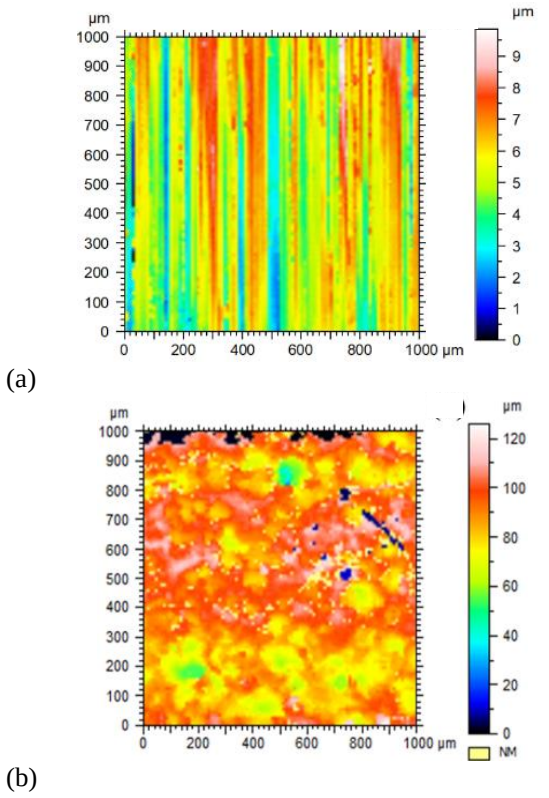

Fig. 2 Surface roughness profile of Al-Si alloy surface: (a) Ra = 1.12 μm; (b) Ra = 17.69 μm

Table 2 Fuel mass, mass flow rate and volume flow rate with different conditions

P_i(MPa), t_i, (ms)	Fuel mass (mg)	Mass flow rate (10^{-3}Kg/s)	Volume flow rate ($10^{-6}m^3$/s)
60,1	8.092	8.092	9.728
60,2	19.075	9.538	11.467
60,3	30.058	10.019	12.045
80,1	10.193	10.193	12.254
80,2	23.226	11.613	13.961
80,3	36.259	12.086	14.529

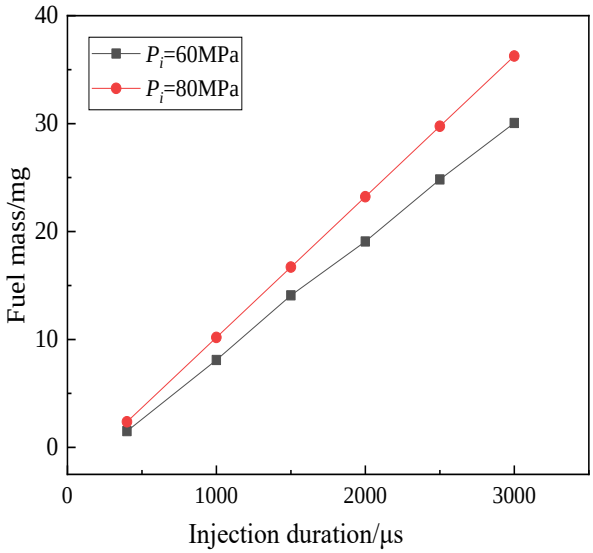

Fig. 3 Fuel injection mass calibration

As the main dynamic force in the spray impingement, the injection pressure directly affects the impingement morphology and the fuel film evolution process (Shi et al., 2020a). However, the injection pressure during cold start at low temperatures is usually maintained at a lower value than that during normal operation. In other words, injection pressure was not a major variable in this study. He et al. (2023) reported that 80 MPa was a more appropriate injection pressure under cold starting conditions which can reduce the ignition delay time (IDT). Thus, our study focused on the combined effects of injection pressure (P_i=60 MPa and 80 MPa (mainly)) and injection duration (t_i=1, 2, and 3 ms). With the intention of providing basic data for the theoretical calculation of the oil film area, a standard injection rate measuring device (produced by EFS) was utilized to calibrate the injection mass under the different injection pulse widths and each injection pressure. Figure 3 exhibits the change rule of injection fuel mass at various injection pressures and injection duration. Table 2 lists the calculation results of the average mass flow rate and volume flow rate based on the injected fuel mass under various injections. Depending on the operating conditions of the engine, the distance from the nozzle to the surface was set as 40 mm. Considering that the compression ignition (CI) characteristics of diesel engines resulted in the misfire phenomenon during the stage of cold start, the change of fuel film after multiple injections was also adopted as a research factor. The injection interval time was set at 150 ms with reference to the idling stage.

2.3 Image Processing Procedure

The original images were processed by MATLAB software and the procedure was performed (Fig. 3) to obtain the liquid phase parameters after spray impingement. Regarding background removal, the first image without spray was defined as a background one, and the first frame image was then subtracted from each frame image. Besides, noise reduction was conducted because there were still some noise points after the process of background removal. Then, an appropriate threshold value was selected, and the gray value of pixel points (less than the threshold value) was set to zero to obtain the processed spray image. This Gaussian filtering was applied to eliminate Gaussian noise in this paper. It replaced the value of the target pixel with the weighted average gray value of the target pixel and its neighboring pixels, representing a type of linear smoothing signal filtering. The Gaussian filtering algorithm was straightforward. It eliminated image noise while protecting image edges through weight analysis.

Binary processing and parameter acquisition were conducted since it was necessary to use the fuel film formed by the initial spray impact as a condition for calculations in sections 3.1 and 3.2. Therefore, a series of images were binarized, and then the spray morphology involving initial fuel film radius (R_0), penetration (P_L), diameter (D_L), and height (H_L) in the image were recorded by edge capture extraction, as shown in Figs. 4 and 5. False color image, images after the noise reduction had been transformed into matching grey-scale pictures, and the false-color image was created by the method of corresponding pixel mapping. The concentration distribution of the liquid phase of the spray was seen more clearly because of the false color.

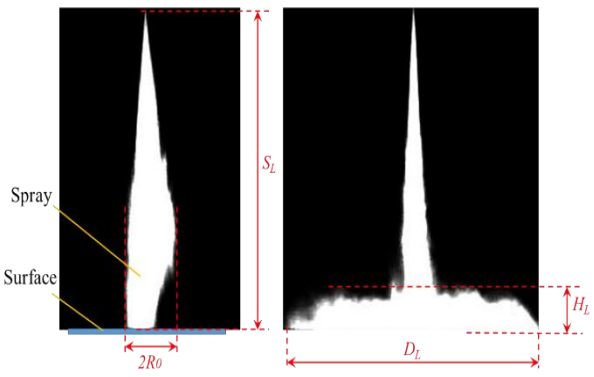

Fig. 4 Captured procedure for the spray morphology

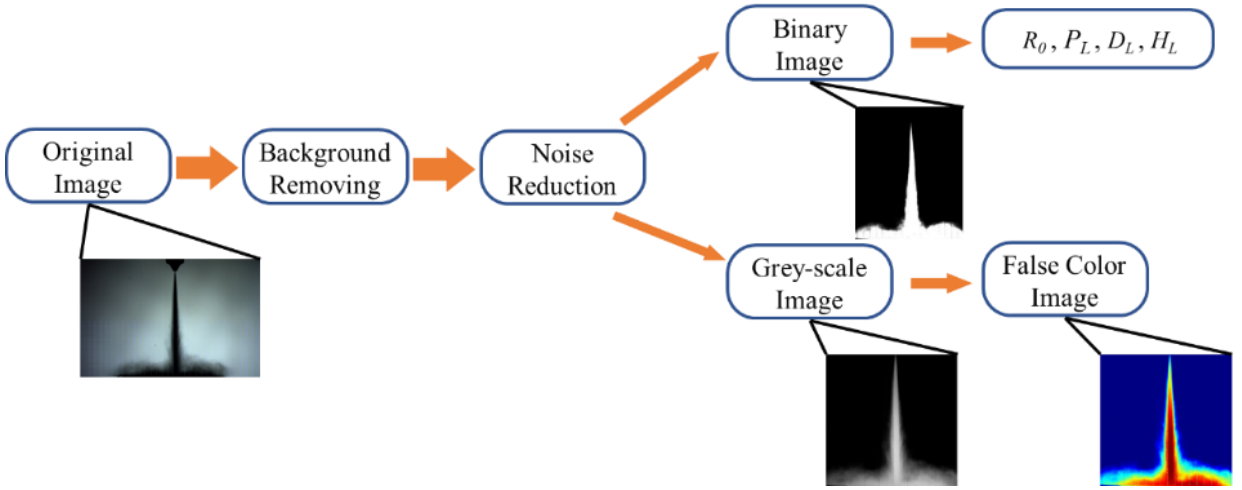

Fig. 5 Image processing procedure for spray impingement obtained by the backlight method

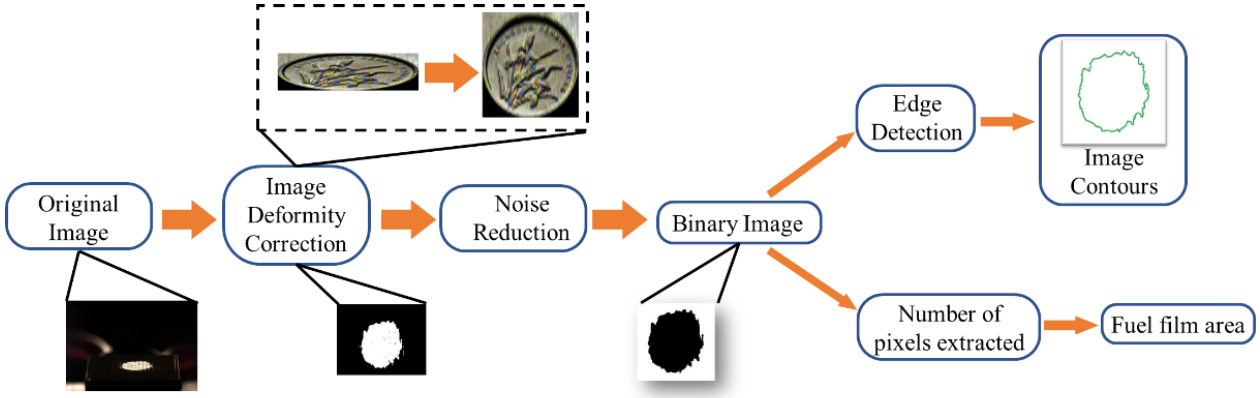

Fig. 6 Processing procedure for the image of fuel film

The morphology of the fuel film was recorded by the scattering method with an inclined camera. Therefore, it was necessary to reconstruct the tilted image of the fuel film by a suitable method. For image deformity correction, the adjustment was made through the original calibration object, as illustrated in Fig. 6. The original inclined image was recovered by adjusting the proportion of vertical coordinates in the image. Specifically, the aspect ratio of the calibrated items in the calibrated image was consistent with the actual aspect ratio. Then, the fuel film image was adjusted in the same way. The recovered image from the background removal process was cropped to the appropriate size. Additionally, the part of noise reduction and binary image was treated similarly to the process of spray impingement. In the part of edge detection, fuel film edges were captured by the canny edge capture algorithm for subsequent comparison. The canny edge capture algorithm was a multi-stage algorithm that performed edge detection by applying Gaussian filtering to remove noise and calculated the gradient magnitude and direction, non-maximum suppression, double threshold detection, and edge tracking. The fuel film area was calculated as the product of the total pixel number of the fuel film domain and the area of a unit pixel. Furthermore, the experimental error was minimized by finding the average value of the measured parameter during three tests.

3. RESULTS AND DISCUSSION

3.1 The Effect of Surface Temperature

An example of spray impacting on the surface was depicted in Fig. 7, with a surface roughness of Ra=1.12 μm and a fuel pressure of P_i=80 MPa. Two different surface temperatures, T_s=-20 °C and 20 °C (room temperature), and injection durations (t_i), t_i =2 ms and 3 ms, were reported. As observed, the phenomena after spray impacting on surfaces with different temperatures only exhibited comparable effects, whereas the fuel film region significantly decreased as T_s became lower.

The fuel film region significantly increased with the prolonged injection duration, as presented in Fig. 7. The spray concentration was higher in the near-wall region at 2ms after the start of injection (ASOI). Longer injection duration led to an increase in the interaction time of the spray and the surface, and more fuel droplets impacted on the surface. At ASOI 3 ms, the spray concentration remarkably reduced with t_i =2 ms, while the greater concentration was still observed with t_i =3 ms. Notably, the fuel film mainly spread from center to outward, even though the near-wall region possessed a higher spray concentration. This was mainly because the spray plume,

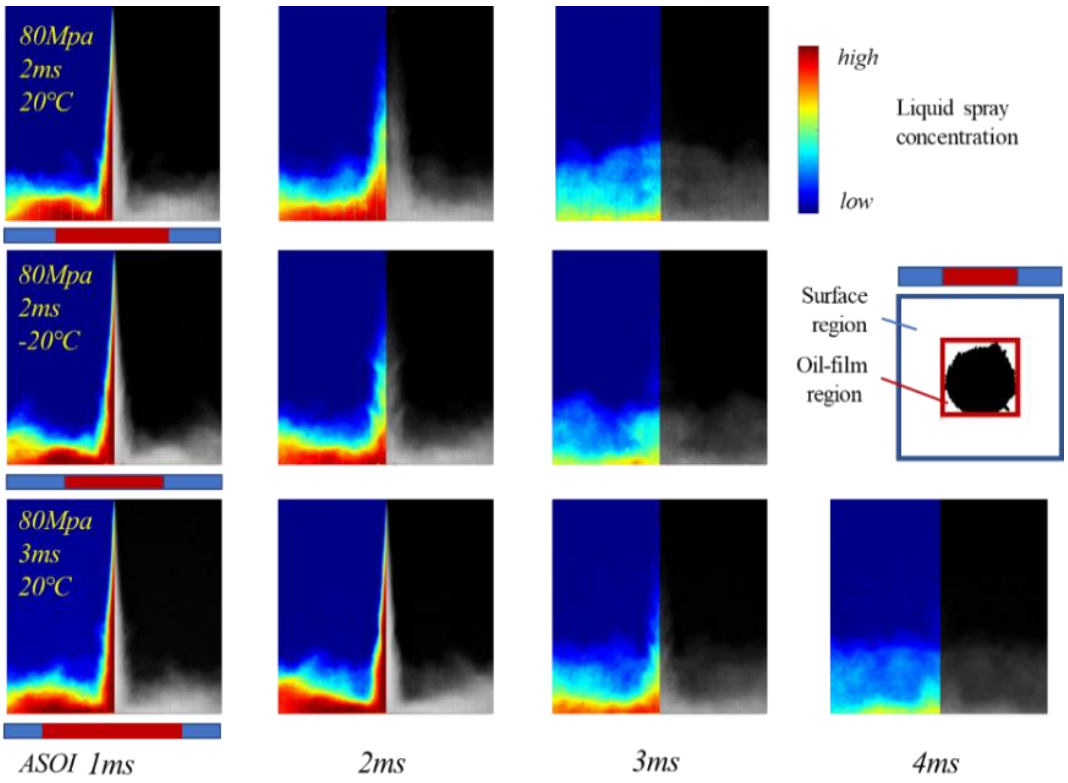

Fig. 7 Distribution of liquid phase after spray impacting on surface at with different *Ts* and *ti* at P_i=80 MPa

not the wall jet, was the position where the oil film quality originated (Liu et al., 2019a).

The influence of surface temperature on the liquid-phase impinging spray was investigated at different values of t_i (Fig. 8). The injection pressure generated by the common rail system provided enough momentum for the spray, contributing to the rapidly boosted expansion of the spray. The P_L and D_L raised immediately, as exhibited in the first two columns of Fig. 8. Due to the hindering effect of the surface, the increasing trend of the P_L gradually decreased at 0.25ms ASOI, while the exact opposite trend was observed for the D_L. The expansion of the spray parallel to the surface was significantly enhanced by surface effects. Consequently, the spray momentum in the vertical surface direction was converted into two jets parallel to the surface. The momentum provided by the injection pressure dominated at this stage, and the surface temperature had barely any effect on the P_L and D_L. The liquid-phase spray was floated by the interaction of the impingement spray and the surrounding air. Nonetheless, the H_L was less than that at ambient conditions. Droplets carried by the spray impacted the surface and quickly formed a fuel film, which had a lower average temperature and higher viscosity on the ultracold surface. The number of droplets in the vortex region decreased owing to the evident phenomenon of adhere and velocity reduction. The H_L reduced with the lower surface temperature in the macroscopic view. The surface temperature exerted more effect on the fuel film than the liquid spray morphology reflected by the P_L, D_L, and H_L.

Figures 8(a) and (b) illustrate visual changes in the spreading fuel film. The fuel film area decreased by about 26 % with the T_s ranging from 20 °C to -20 °C, at P_i =60 MPa, t_i =3 ms. The spreading fuel film after spray impacting was composed of tiny deposing droplets not atomized. During the early stage of injection, the first droplets were piling up to create a liquid film. Once the fuel film was created, the spreading of the liquid film was mainly driven by the high-speed flow of spray. The force of spreading was provided by the pressure difference and the shear stress of high-velocity-induced airflow. The effect of viscosity hindered the spreading of fuel film. The heat exchange occurring between the ultracold surface and the tiny droplets provoked a decrease in the film temperature and an increase in its viscosity, preventing the film from spreading.

Regarding the cases reported in Fig. 9, the fuel film area (S) at P_i =60 MPa, T_s =20 °C stabilized to S≈210 mm^2 and S≈490 mm^2 for t_i =1 ms and 3 ms, respectively. Moreover, digitations were observed at the edge of the fuel film, whereas their size always remained smaller compared to the film. This phenomenon was mainly determined by spray spatial non-uniformity, and the wavy patterns were affected by the non-uniformity during injection (Xiao et al., 2019). Although the fuel pressure P_i =80 MPa demonstrated a similar pattern, the effect of surface temperature was lessened, as exhibited in Fig. 10. The fuel film area decreased by about 20 % at P_i =80 MPa, t_i =3 ms. The heat transfer was enhanced by higher fuel pressure, while the higher pressure also provided the higher shear stress of the air-fuel flow and more fuel-impacting mass. The rise in fuel pressure finally weakened the effect of the ultracold surface and reinforced the spreading of the fuel film.

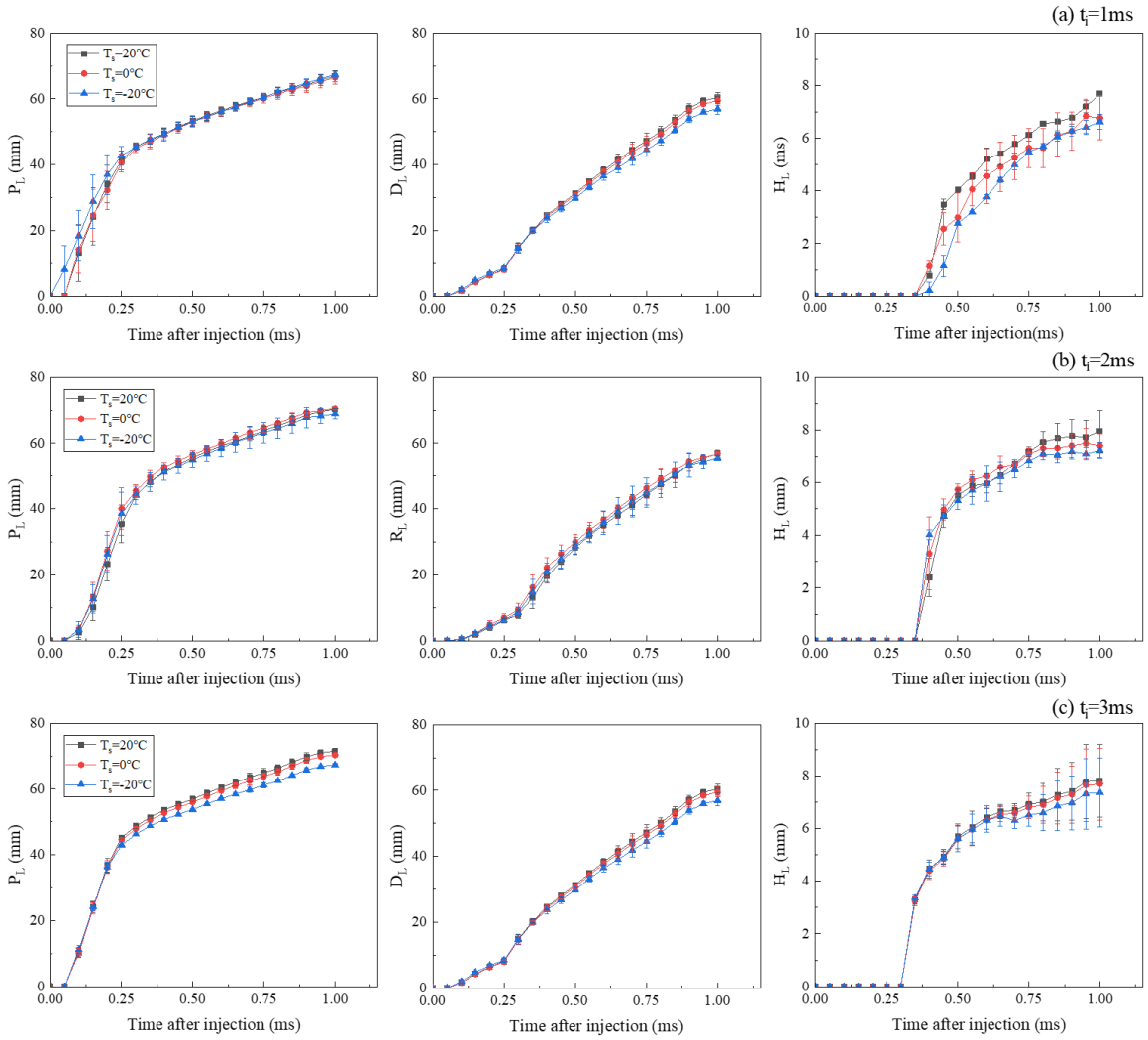

Fig. 8 Distribution of liquid phase after spray impacting on surface with different *Ts* and t_i at P_i=80MPa

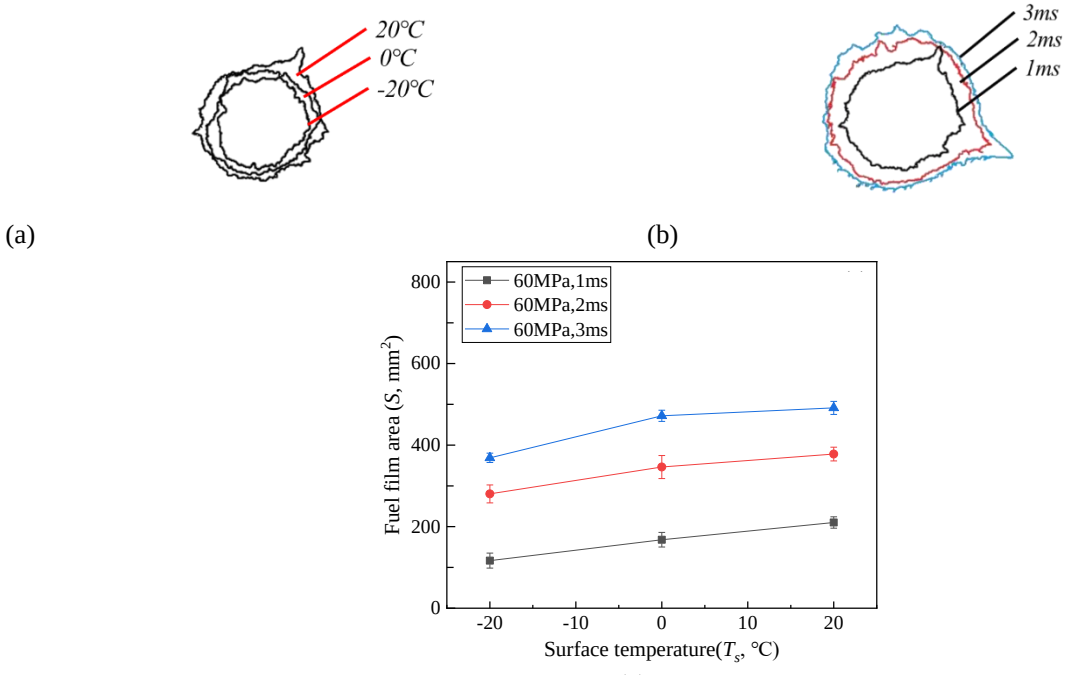

Fig. 9 Fuel films changed with different *Ts* and t_i at P_i =60 MPa; (a) Film outlines with different *Ts* at t=1 ms; (b) Film outlines with different t_i at *Ts* =20 ℃; (c) Film areas with different *Ts* and t_i;

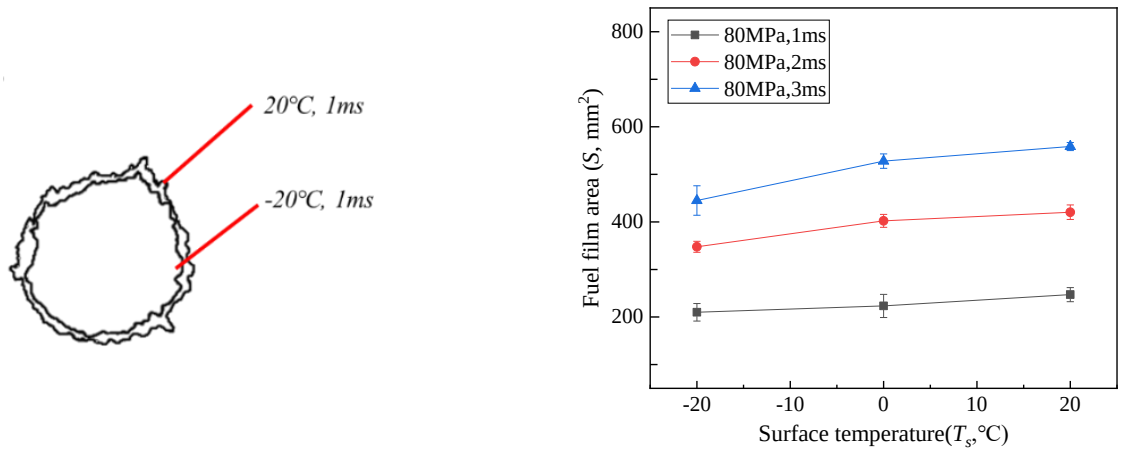

(a) (b)

Fig. 10 Fuel films changed with different *Ts* and *ti* at *Pi*=80 MPa; (a) Film outlines with different *Ts*; (b) Film areas with different *Ts* and *ti*;

3.2 Empirical Correlation of Fuel Film Area

The process between spray and surface is a complex process involving heat transfer and momentum change, in which a large of high-speed tiny droplets impact on the surface (Luo et al., 2021). The following assumptions were established under isothermal conditions. Droplets after spray impacting on the surface were divided into two parts as follows. Part of them adhered or stuck on the surface to form a liquid film, and the other part escaped from the surface by bouncing, splashing, or breakup. The actual process was more intricate than the assumption. Nevertheless, the fuel film formation was remarkedly dependent on deposited droplets. Mass conservation of the spreading fuel film can be expressed as:

$$\pi R^2 h \approx k_m Q t \tag{1}$$

where R represents the equivalent radius of the fuel film. The fuel film shape was simplified to a pizza shape, with an equivalent uniform thickness represented by h, as demonstrated in Fig. 1. Besides, k_m denotes the deposition coefficient; indicates the mass proportion of fuel film to total spray mass; Q signifies the injection discharge of the injector; t stands for interaction time between spray and surface. With respect to the analysis in Section 3.1, the spreading of fuel film was induced by the pressure gradient and balanced by viscous friction. Contributions of capillary pressure, inertia, and friction at the contact line were neglected compared to the effect of the pressure gradient and viscosity (De Gennes, 1985; Lamiel et al., 2021). The momentum balance in the film can be simplified to:

$$\frac{\Delta P}{R} \approx \frac{\mu V_R}{h^2} \tag{2}$$

Where ΔP represents the pressure gradient that depends on injection pressure (P_i), hence $\Delta P = K_P P_i$. Among them, K_P indicates pressure loss coefficient. This was primarily a wall jet driving the spreading of the oil film after spray impacting on the surface. The driving force stemmed from the pressure gradient ΔP that was strengthened with the injection pressure P_i. V_R represents the spreading velocity of the front surface of the fuel film, is expressed by the first derivative between the equivalent radius of the liquid film (R) and interaction time (t), dR/dt. This was primarily because V_R depended mainly on the expansion of the fuel film equivalent radius with interaction time t. Consequently, Eq. 3 can be determined:

$$R^2 V_R = \pi^{-2} k_P P_i k_m^2 Q^2 \mu^{-1} t^2 \tag{3}$$

The equivalent radius of the liquid film R can be obtained as follows using Eq. 3:

$$R^2 = (2\pi^{-2} k_P P_i k_m^2 Q^2 \mu^{-1})^{1/3} t + R_0^2 \tag{4}$$

Where R_0 represents the initial oil film radius by the initial spray impacting. Thus, the fuel film area (S) can be expressed as:

$$S = \pi R^2 = (2\pi k_P P_i k_m^2 Q^2 \mu^{-1})^{1/3} t + \pi R_0^2 \tag{5}$$

The fitting result was performed through the data from this study, as depicted in Fig. 11. Although the effect of the relaxation process was neglected in this analysis, the empirical correlation value corresponded well to the experimental value. This was fundamentally provoked by the higher viscosity of the fuel and the rapid dissipation of momentum at the end of

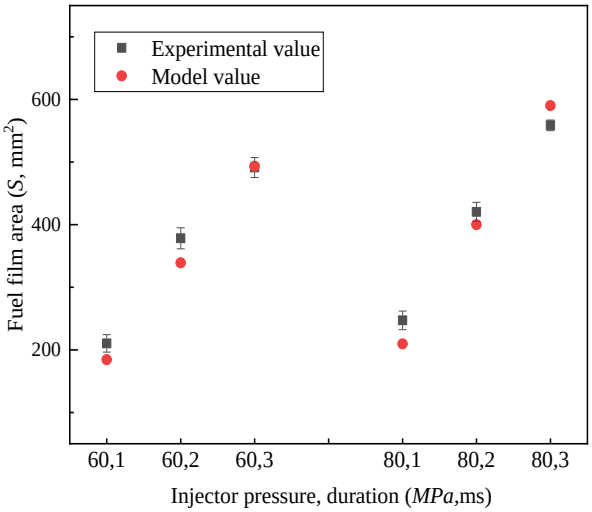

Fig. 11 Comparison of experiment and empirical correlation under isothermal conditions

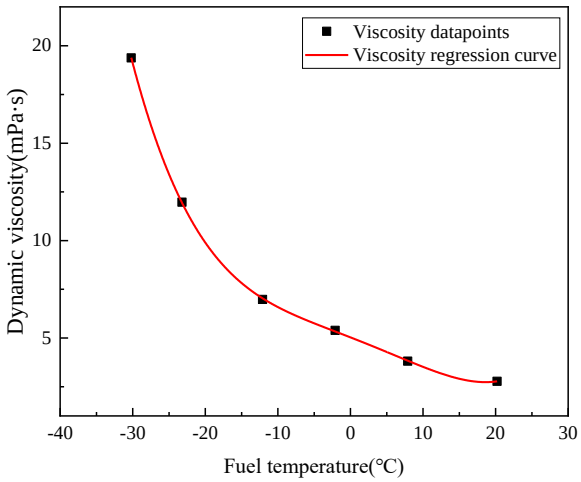

Fig. 12 Dynamic viscosity of fuel changes with fuel temperature

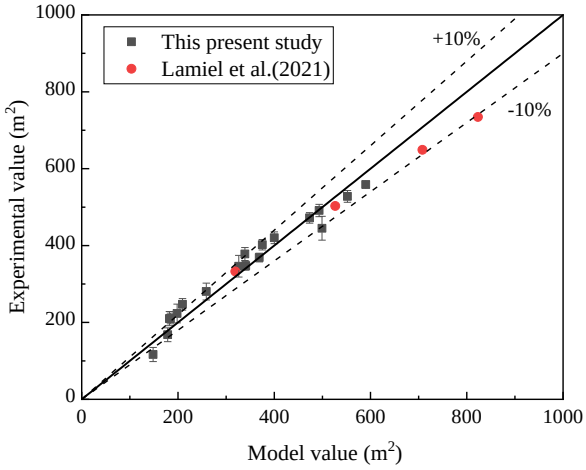

Fig. 13 Comparison of experimental and model values of fuel film area with different conditions;

the interaction period. The fitting result demonstrated that $k_m^2 k_P = 1.45 \times 10^{-4}$, and the range of k_m varied from 0.2 to 0.6, which was based on studies of Schulz and Beyrau (2018), Ko and Arai (2002), and Akop et al. (2013). The study condition of Akop et al. (2013) was more similar to this experiment, thus k_m≈0.38, P_i=60 MPa and k_m≈0.35, P_i=80 MPa. Considering the k_m with different injection pressures, $k_P = 1.01 \times 10^{-3}$ and 1.19×10^{-3} were calculated. All of the results were smaller than those obtained by Lamiel et al. (2021). This reflects the weakened effect of pressure gradient driven by higher injection pressure. The deposition coefficient (k_m) may change with the different fuel temperatures because of the physical properties, whereas the coefficient was considered constant for this investigation. Nonetheless, this coefficient was close to the mean value obtained by Xiao et al. (2021) at different experimental conditions.

The higher viscosity of the fuel film with the low temperature hindered the film spreading. Borman and Nishiwaki (1987) suggested that the efficiency of heat transfer during spray impacting on the surface was mainly determined by the temperature difference between the fuel and the surface, as well as the strength of the heat transfer. The strength of heat transfer depends on a combination of factors such as injection pressure and fuel type. For the purpose of simplifying this problem, the uneven temperature distribution in the film was considered; meanwhile, a uniform equivalent temperature (T_e) was assumed at the film and calculated as follows:

$$T_e = T_{f,20} - k_T(T_{f,20} - T_s) \tag{6}$$

Where $T_{f,20}$ represents the fuel temperature at room temperature, which was 20°C in this study; k_T indicates the strength of heat transfer. The thermophysical properties of fuel changed with different ambient temperatures, especially viscosity. As fuel temperature decreased, the dynamic viscosity ($\mu(T_f)$) significantly rose, as illustrated in Fig. 12. Meanwhile, the trend of dynamic viscosity was expressed by a 4-order power function (Eq. (7)). The regression coefficient was R^2 = 0.999.

$$\begin{aligned}\mu(T_f) = 5.03 &- (0.15 \times T_f) \\ &- (8.02 \times 10^{-4} \times T_f^2) \\ &- (8.29 \times 10^{-5} \times T_f^3) \\ &+ (1.01 \times 10^{-5} \times T_f^4)\end{aligned} \tag{7}$$

Accordingly, the fuel film area (S) at different surface temperatures can be expressed as follows:

$$S(T_e) = \pi R^2 = (2\pi k_P P_i k_m^2 Q^2 \mu(T_e)^{-1})^{1/3} t + \pi R_0^2 \tag{8}$$

The fitting coefficients derived based on Eq. (6), Eq. (7), and Eq. (8) were listed in Table 3, which demonstrates the consistency of the fitted relationship. The fuel film area with different conditions was reflected by the empirical correlation, as illustrated in Fig. 13. The model can accurately unveil the trend of fuel film area change, with an overall deviation within ±10%. The main reason for the deviation of the model is that some factors are ignored in the empirical relation to simplify the calculation, and the actual spray wall collision process is more complicated.

3.3 The Effect of Surface Roughness

The surface roughness was changed by the thermal shock after the impacting flame and carbon deposition due to poor combustion at the cold start conditions. Figures 14 (a) and (b) visualize the decreasing area of the fuel film with the increasing roughness. However, the area was affected by surface temperatures (T_s) and injection durations (t_i). The fuel film area after spray impacting on the ultra-cold surface

Table 3 k_T for different P_i and T_s

P_i(MPa), T_s, (°C)	60/80, 20	60, 0	60, -20	80, 0	80, -20
k_T for different P_i and T_s	0	0.320	0.823	0.395	0.415
Adjust R-Square	0.995	0.998	0.993	0.994	0.991

decreased remarkably. When the injection duration was 1ms, the fuel film area decreased by about 13 % with *Ra* changing from 1.12 μm to 17.69 μm at T_s =20 °C, but the fuel area dropped by about 28% at T_s =-20 °C, as illustrated in Fig. 13. The surface roughness played an imperative role in the process of fuel film spreading, and this effect was magnified on the ultra-cold surface. The increase in the surface roughness, as well as the greater contact area between the fuel film and the surface, reinforced the heat transfer and lowered the film temperature. As a result, the film area decreased even more significantly under this effect.

When the surface temperature was 20 °C, the fuel film area decreased by about 7 % and 13 % at t_i=3 ms and t_i=1 ms, respectively, as presented in Fig. 14(c). The surface became more uneven as the surface roughness increased (Fig. 2). The thickness of the fuel film after spray impacting on the surface is typically in the micron range (He et al., 2020). Therefore, the obstruction at the contact line by the rougher surface was more noticeable during the spreading process. Nonetheless, the higher injection mass induced by the longer injection durations weakened the effect of the surface roughness. This effect of the higher injection duration also occurred on the ultra-cold surface. When the surface temperature dropped from 20 °C to -20 °C, the reduction ratio of fuel film area increased from 13 % to 28 % with the higher *Ra* at t_i=1 ms and P_i=80 MPa, and the reduction ratio rose from 7 % to 10 % at t_i=3 ms.

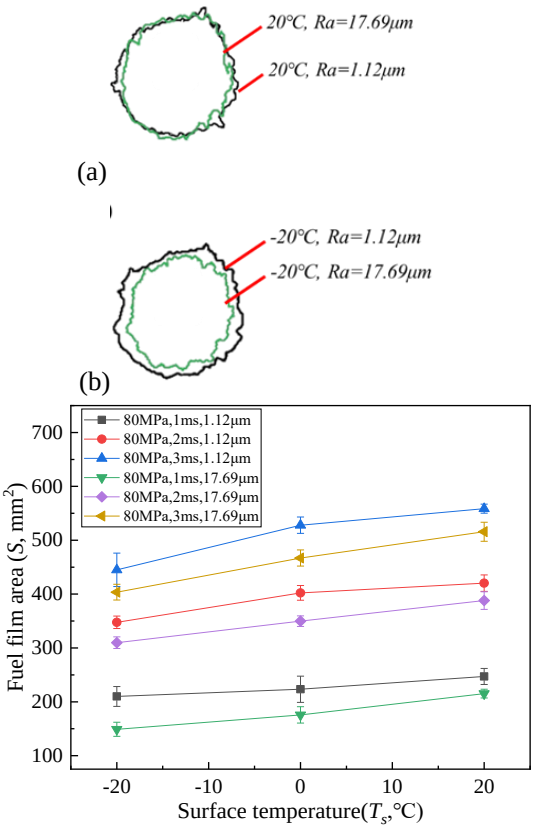

Fig. 14 Fuel films changed with different *Ra* and *Ts* at P_i=80 MPa; (a) and (b) Film outlined (t_i =1 ms) with different *Ra* at *Ts*=20 °C and -20 °C, respectively; (c) Film areas changed with different *Ra* and *Ts*

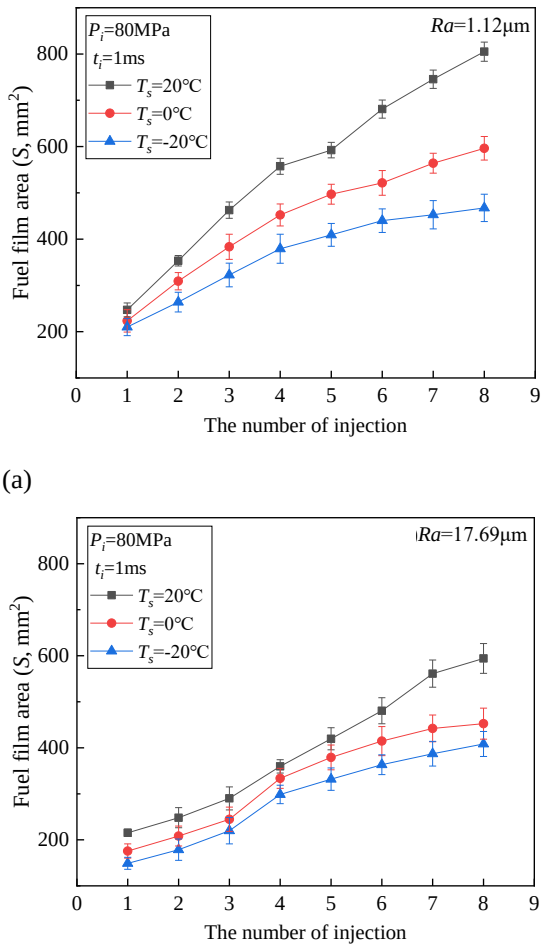

Fig. 15 Fuel film areas changed with the number of injections; (a) The area changes with different *Ts* at *Ra*=1.12 μm; (b) The area changes with different *Ts* at *Ra*=17.69 μm

3.4 The Effect of Surface Roughness

The phenomenon of a misfire for diesel engines during cold starting at low temperatures occurred highly frequently owing to the poor atomization and the low-temperature surface. Therefore, the fuel film consisting of unevaporated droplets accumulated after spray impacting on the surface. The fuel film edge exceeded the observation window because of the film accumulation by the continuous multiple injections at long injection durations (t_i=2 ms and 3 ms). Thus, the injection duration (t_i=1 ms) was selected to curtail the film area statistical error in this section, as demonstrated in Fig. 15.

The fuel film area continuously increased with the number of injections, and the area increasing rate was affected by the surface temperature (Fig. 15(a)). The fuel film area decreased by about 15 % as T_s changed from 20 °C to -20 °C at the first injection stage. The oil film area increased with continuous accumulation. In the fourth injection stage, for instance, the area of the oil film expended to about 557 mm^2 at T_s =20 °C. Correspondingly, the area of the oil film was enlarged but was only 379 mm^2 at T_s =-20 °C, demonstrating a difference of nearly 32 % with T_s varying from 20 °C to -20 °C. The film area after spray impacting on an ultra-cold surface accumulated more slowly as the

number of injections further increased. At the 8th injection stage, the area increased by about 15 mm^2 compared to the 7th injection stage. Notably, the surface was dry before the spray impacting, and the spray impacted on the wet surface after the first spray. Therefore, the film area was more affected by the previously accumulated fuel film. The deposited area of fuel film after spray impacting on wet surface considerably decreased with the higher viscosity and depth of the initial liquid film on the surface (Wang et al., 2021). In this study, the heat transfer between the fuel film and the ultra-cold surface provoked the boosted film viscosity, leading to the decreased film area and higher film thickness. The fuel film difference indicated by the film area became more noticeable with the increasing injection times. Moreover, the accumulation of oil film in the diesel engine cylinder after misfire brought about higher emissions or damage from excessive thermal shock after subsequent normal operation.

The accumulated area of fuel film significantly varied at the higher surface roughness (Ra=17.69 μm). From the first injection to the third injection, the growth area of the fuel film at T_s =20 °C was similar to that at T_s =-20 °C. The film area was substantially smaller than that formed on the surface with low roughness (Ra=1.12 μm), and the difference in the area at different T_s did not change appreciably (Fig. 15). The localized peaks on the surface had a similar spatial scale to the fuel film thickness. Therefore, the combination of the residual fuel film on the surface and the surface roughness influenced the spreading of the fuel. With the increasing number of injections (after the fourth injection), the trend of film area on the high roughness surface approached that on the low roughness surfaces. This can be explained as follows. The accumulation of fuel film weakened the effect of surface roughness, and the film spreading was mainly influenced by the viscosity and thickness of the fuel film.

4. CONCLUSION

In this paper, our research group designed a test matrix to determine the influence of various parameters, such as surface temperature, injection pressure, injection duration, and surface roughness, on the spray impingement and fuel film spreading process. The phenomena observed after spray impacting on different low-temperature surfaces exhibited comparable effects. The penetration and diameter of the impinging spray were not affected by the low surface temperature attributed to the ample momentum, while the height decreased on the ultra-cold surface. Nonetheless, the fuel film region significantly decreased with lower surface temperature and shorter injection durations. The heat transfer between the fuel film and the low-temperature surface contributed to the boosted film viscosity, thereby hindering the spreading of the fuel film. Shorter injection durations provoked the lessened mass of the fuel spray deposited and the curtailed film spreading area. An empirical correlation of the fuel film area, which better reflected the relationship between the fuel film area and the surface temperature or injection conditions, was established through the analysis of momentum conservation and qualitative temperature assessments. The decrease in the fuel film area was more noticeable on the surface with lower temperatures and higher surface roughness (*Ra*=17.69 μm). Nevertheless, this trend was mitigated by longer injection durations. The greater injection mass was stimulated by the longer injection durations, reducing the obstruction caused by higher surface roughness and ultra-cold surfaces to fuel film spreading. Furthermore, the fuel film area was enlarged with the increasing number of injections, whereas the growth trend was considerably influenced by surface temperature roughness. The fuel film area on the ultra-cold surfaces expanded more slowly with the rising number of injections ascribed to the higher viscosity and thickness of the previous residual film.

ACKNOWLEDGMENTS

This research was financially supported by the National Key R&D Project of China (Grant No. 2022-XXXX-XX-180-00).

CONFLICT OF INTEREST

The authors declare that they have no conflict of interest or competing interests.

AUTHORS CONTRIBUTION

Shuang Jin: Drafting of manuscript, Data Processing, Results analysis; **Weizheng Zhang:** Research Initiation, Data Processing; **Zhenyao Guo:** Detailed Discussion, Result Analysis; **Yanpeng Yuan:** Experiment execution, Data Processing; **Yuwei Liu and Jie Yan:** Reviewing, and editing.

REFERENCES

Abou Al-Sood, M. M., Abdel-Latif, A. A., & Ibrahim, A. M. (1999). Optimum compression ratio variation of a 4-stroke, direct injection diesel engine for minimum bsfc (No. 1999-01-2519). *SAE Technical* Paper. https://doi.org/10.4271/1999-01-2519

Akop, M. Z., Zama, Y., Furuhata, T., & Arai, M. (2013). Experimental investigations on adhered fuel and impinging diesel spray normal to a wall. *Atomization and Sprays*, 23(3). https://doi.org/10.1615/AtomizSpr.2013007447

Borman, G., & Nishiwaki, K. (1987). Internal-combustion engine heat transfer. *Progress in Energy and Combustion Science*, *13*(1), 1-46. https://doi.org/10.1016/0360-1285(87)90005-0

Chen, R., Nishida, K., & Shi, B. (2020). Quantitative measurement of mixture formation in an impinging spray of ethanol-gasoline blend under cold-start condition via UV–Vis dual-wavelength laser absorption scattering (LAS) technique. *Fuel*, *262*, 116685. https://doi.org/10.1016/j.fuel.2019.116685

Cho, K., Grover Jr, R. O., Assanis, D., Filipi, Z., Szekely, G., Najt, P., & Rask, R. (2010). Combining instantaneous temperature measurements and CFD for analysis of fuel impingement on the DISI engine piston top. *Journal of Engineering for Gas Turbines*

and Power, *132*(7), 072805. https://doi.org/10.1115/1.4000293

De Gennes, P. G. (1985). Wetting: statics and dynamics. *Reviews of Modern Physics*, *57*(3), 827. https://doi.org/10.1103/RevModPhys.57.827

Drake, M. C., Fansler, T. D., Solomon, A. S., & Szekely Jr, G. A. (2003). Piston fuel films as a source of smoke and hydrocarbon emissions from a wall-controlled spark-ignited direct-injection engine. *SAE Transactions*, 762-783. https://www.jstor.org/stable/44741311

Egermann, J., Taschek, M., & Leipertz, A. (2002). Spray/wall interaction influences on the diesel engine mixture formation process investigated by spontaneous Raman scattering. *Proceedings of The Combustion Institute*, *29*(1), 617-623. https://doi.org/10.1016/S1540-7489(02)80079-7

He, X., Li, Y., Liu, C., Sjöberg, M., Vuilleumier, D., Liu, F., & Yang, Q. (2020). Characteristics of spray and wall wetting under flash-boiling and non-flashing conditions at varying ambient pressures. *Fuel*, *264*, 116683. https://doi.org/10.1016/j.fuel.2019.116683

He, X., Xu, K., Liu, Y. L., Zhang, Z., Zhang, H., & Zhao, J. (2023). Effects of ambient density and injection pressure on ignition and combustion characteristics in diesel spray under plateau cold-start conditions. *Fuel*, *352*, 129039. https://doi.org/10.1016/j.fuel.2023.129039

Hwang, J., Park, Y., Bae, C., Lee, J., & Pyo, S. (2015). Fuel temperature influence on spray and combustion characteristics in a constant volume combustion chamber (CVCC) under simulated engine operating conditions. *Fuel*, *160*, 424-433. https://doi.org/10.1016/j.fuel.2015.08.004

Ko, K., & Arai, M. (2002). Diesel spray impinging on a flat wall, part i: Characteristics of adhered fuel film in an impingement diesel spray. *Atomization and Sprays*, *12*(5&6). https://doi.org/10.1615/AtomizSpr.v12.i56.120

Lamiel, Q., Lamarque, N., Hélie, J., & Legendre, D. (2021). On the spreading of high-pressure spray-generated liquid wall films. *International Journal of Multiphase Flow*, *139*, 103619. https://doi.org/10.1016/j.ijmultiphaseflow.2021.103619

Li, X., Pan, H., Dong, X., Hung, D., & Xu, M. (2019). Spray impingement wall film breakup by wave entrainment. *Proceedings of the Combustion Institute*, *37*(3), 3287-3294. https://doi.org/10.1016/j.proci.2018.07.101

Liu, H., Chen, B., Feng, L., Wang, Y., Yi, W., & Yao, M. (2018). Study on fuel distribution of wall-impinging diesel spray under different wall temperatures by laser-induced exciplex fluorescence (LIEF). *Energies*, *11*(5), 1249. https://doi.org/10.3390/en11051249

Liu, Y., Pei, Y., Guo, R., Wang, C., & Xu, B. (2019a). Investigation of the liquid fuel film from GDI spray impingement on a heated surface with the laser induced fluorescence technique. *Fuel*, *250*, 211-217. https://doi.org/10.1016/j.fuel.2019.03.120

Liu, H., Wang, J., Duan, H., Cai, C., Jia, M., & Zhang, Y. (2019b). Experimental study on the boiling criterion of the fuel film formed from spray/wall impingement. *Experiments in Fluids*, *60*, 1-14. https://doi.org/10.1007/s00348-019-2829-8

Luo, H., Jin, Y., Nishida, K., Ogata, Y., Yao, J., & Chen, R. (2021). Microscopic characteristics of impinging spray sliced by a cone structure under increased injection pressures. *Fuel*, *284*, 119033. https://doi.org/10.1016/j.fuel.2020.119033

Meingast, U., Staudt, M., Reichelt, L., Renz, U., & Sommerhoff, F. A. (2000). Analysis of spray/wall interaction under diesel engine conditions. *SAE Transactions*, 299-312. https://www.jstor.org/stable/44634220

Pan, H., Xiao, D., Hung, D., Xu, M., & Li, X. (2019). Experimental investigations of wall jet droplet impact on spray impingement fuel film formation. *Fuel*, *241*, 33-41. https://doi.org/10.1016/j.fuel.2018.12.021

Pan, H., Xu, M., Hung, D., Lv, H., Dong, X., Kuo, T. W., & Parrish, S. E. (2017). Experimental investigation of fuel film characteristics of ethanol impinging spray at ultra-low temperature (No. 2017-01-0851). *SAE Technical Paper*. https://doi.org/10.4271/2017-01-0851

Oruganti, S. K., Torelli, R., Kim, K. S., Mayhew, E., & Kweon, C. B. (2024). A Phenomenological Thermal Spray Wall Interaction Modeling Framework Applied to a High-Temperature Ignition Assistant Device. *Journal of Engineering for Gas Turbines and Power*, *146*(9).

Schulz, F., & Beyrau, F. (2018). Systematic investigation of fuel film evaporation (No. 2018-01-0310). *SAE Technical Paper*. https://doi.org/10.4271/2018-01-0310

Schünemann, E., Fedrow, S., & Leipertz, A. (1998). Droplet size and velocity measurements for the characterization of a DI-diesel spray impinging on a flat wall. *SAE Transactions*, 1305-1313. https://www.jstor.org/stable/44746541

Shi, Z., Cao, W., Wu, H., Li, H., Zhang, L., Bo, Y., & Li, X. (2022). Research on destructive knock combustion mechanism of heavy-duty diesel engine at low temperatures. *Combustion Science and Technology*, 1-24. https://doi.org/10.1080/00102202.2022.2156790

Shi, Z., Lee, C. F., Wu, H., Li, H., Wu, Y., Zhang, L., & Liu, F. (2020a). Effect of injection pressure on the impinging spray and ignition characteristics of the heavy-duty diesel engine under low-temperature conditions. *Applied Energy*, *262*, 114552. https://doi.org/10.1016/j.apenergy.2020.114552

Shi, Z., Lee, C. F., Wu, H., Li, H., Wu, Y., Zhang, L., &

Liu, F. (2020b). Visualization research on low-temperature ignition and combustion characteristics of diesel/gasoline blends under cold-start conditions. *Journal of Engineering for Gas Turbines and Power*, *142*(6), 061011. https://doi.org/10.1115/1.4047181

Suh, H. K., Park, S., & Lee, C. S. (2007). A study of the flow and atomization characteristics of impinged diesel spray on a chamber wall. *Atomization and Sprays*, 17(7). https://doi.org/10.1615/AtomizSpr.v17.i7.10

Wang, C., Pei, Y., Qin, J., Peng, Z., Li, X., & Liu, Y. (2022). A quantitative study on deposited fuel film and microscopic droplet characteristics of gasoline surrogate fuel and ethanol spray impingement. *Fuel Processing Technology*, *238*, 107505. https://doi.org/10.1016/j.fuproc.2022.107505

Wang, C., Pei, Y., Qin, J., Peng, Z., Liu, Y., Xu, K., & Ye, Z. (2021). Laser induced fluorescence investigation on deposited fuel film from spray impingement on viscous film over a solid wall. *Energy*, *231*, 120893. https://doi.org/10.1016/j.energy.2021.120893

Wu, H., Cao, W., Li, H., Shi, Z., Zhao, R., Zhang, L., & Li, X. (2023). Wall temperature effects on ignition characteristics of liquid-phase spray impingement for heavy-duty diesel engine at low temperatures. *Combustion Science and Technology*, *195*(3), 456-471. https://doi.org/10.1080/00102202.2021.1961133

Xiao, D., Li, X., Hung, D. L., & Xu, M. (2019). Characteristics of impinging spray and corresponding fuel film under different injection and ambient pressure (No. 2019-01-0277). *SAE Technical Paper*. https://doi.org/10.4271/2019-01-0277

Xiao, D., Qiu, S., Hung, D., Li, X., Nishida, K., & Xu, M. (2021). Evaporation and condensation of flash boiling sprays impinging on a cold surface. *Fuel*, *287*, 119423. https://doi.org/10.1016/j.fuel.2020.119423

Zhang, G., Wu, H., Cao, Z., Li, X., & Myagkov, L. (2023). Coupling effect of thermal conducting and low-temperature reaction process on ignition characteristics under diesel-like conditions. *Fuel*, *340*, 127533. https://doi.org/10.1016/j.fuel.2023.127533

Zhao, M., & Kaiser, S. A. (2018). Optical diagnostics for knock in compression-ignition engines via high-speed imaging. *SAE International Journal of Engines*, *11*(6), 903-918. https://www.jstor.org/stable/26649137

Zhu, G. S., Reitz, R. D., Xin, J., & Takabayashi, T. (2001). Modelling characteristics of gasoline wall films in the intake port of port fuel injection engines. *International Journal of Engine Research*, *2*(4), 231-248. https://doi.org/10.1243/146808701154545

Zhu, J., Nishida, K., & Uemura, T. (2014). Experimental study on flow fields of fuel droplets and ambient gas of diesel spray-free spray and flat-wall impinging spray. *Atomization and Sprays*, *24*(7). https://doi.org/10.1615/AtomizSpr.2014009901